

AURORAL HYDROGEN EMISSION

By R. H. EATHER* and F. JACKA†

[Manuscript received November 22, 1965]

Summary

A photometer using a tilting interference filter to measure auroral hydrogen emission is described, and the method of analysis of records from such a photometer is discussed.

Average $H\beta$ intensities measured at the Australian National Antarctic Research Expeditions station, Mawson, were 25–50 R in a period of low solar activity. Doppler shift of the peak of the magnetic zenith $H\beta$ profile was $6 \pm 1 \text{ \AA}$ over a wide range of conditions of intensity and auroral and magnetic activity. No “narrow profile” auroral hydrogen emission was observed and the auroral hydrogen emission showed no polarization.

The intensity of hydrogen emission was not dependent on the intensity of $\lambda 4709$ or $\lambda 6300 \text{ \AA}$ emissions from visual auroras, nor on the type or intensity of visual auroral forms. However, when visual auroras were not present, a correlation was sometimes observed between changes of intensity in $H\beta$ and $\lambda 4709 \text{ \AA}$ emissions. The hydrogen emission was associated closely with r type E_s ionization. There appeared to be no correlation with magnetic activity or with v.l.f. radiation.

The region of maximum hydrogen emission always appeared equatorwards of visual forms. An equatorwards movement of the zone of emission was observed before midnight; the zone spread back polewards after auroral breakup and then returned equatorwards; a return of the zone polewards was sometimes observed in the morning hours.

An attempt to measure the height of hydrogen emission by the van Rhijn method was unsuccessful but led to a means of selecting the most appropriate of the several published magnetic zenith hydrogen line profiles. Reported asymmetry of magnetic horizon hydrogen line profiles is explained in terms of a wide height distribution of the emission and possible small deviations of the direction of pointing from the true magnetic horizon direction.

I. INTRODUCTION

Following the discovery of the Balmer lines of hydrogen in auroral spectra (Vegard 1939), there has been a considerable number of papers published on this subject. The literature was reviewed by Chamberlain (1961) and Galperin (1963). Relatively little work has been published since.

The present study was undertaken with the aim of resolving some of the major inconsistencies and uncertainties concerning the morphology of the hydrogen emission and its relationship to the visible aurora.

* Antarctic Division, Department of External Affairs, Melbourne, and Physics Department, University of New South Wales, Kensington, N.S.W.; present address: Department of Space Science, Rice University, Houston, Texas, U.S.A.

† Antarctic Division, Department of External Affairs, Melbourne; present address: Mawson Institute for Antarctic Research, University of Adelaide.

Measurements were made from the Australian National Antarctic Research Expeditions station at Mawson ($67\cdot6^{\circ}\text{S.}$, $62\cdot9^{\circ}\text{E.}$), which lies about 2° inside the maximum frequency isoaurora of Bond and Jacka (1962). The $\text{H}\beta$ line profile was scanned by means of a narrow band pass interference filter, tilted periodically relative to the incident light beam. As this technique has not been discussed in the literature, the methods of reduction of the records are described in some detail.

II. INSTRUMENTATION

(a) *The Photometer*

Observations were made with a two-channel photometer, using multilayer interference filters to select the $\text{H}\beta$ line and other spectral lines of interest. The $\text{H}\beta$ line was selected in preference to $\text{H}\alpha$ (even though $\text{H}\alpha$ is stronger) because

- (1) photomultipliers are more sensitive at the shorter wavelength, and
- (2) $\text{H}\beta$ measurements are not as subject to contamination from overlapping emissions.

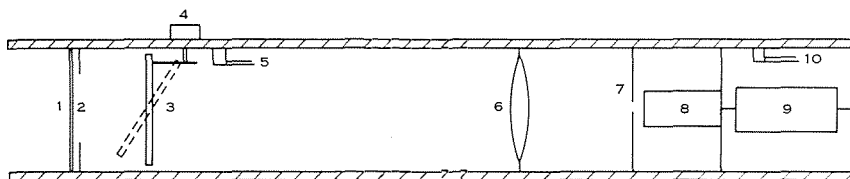


Fig. 1.—Main features of one channel of the photometer (not to scale). 1, Cover glass; 2, aperture; 3, filter; 4, filter rocking motor; 5, thermostat; 6, lens; 7, field stop; 8, photomultiplier; 9, pulse amplifier and ratemeter; 10, thermostat.

The main features of one channel of the photometer are shown in Figure 1. A cover glass prevented snow and cold air from entering the photometer tube. A series of apertures at the entrance pupil (just behind the cover glass) could be used to limit the amount of light entering the photometer; the filter was mounted near the front end of the photometer tube and could be tilted through an angle of 10° by a cam driven by a synchronous motor. The transmitted light passed through a convex lens and was defocused onto the cathode of a photomultiplier tube (E.M.I. type 9558B) at the exit pupil. The field of view could be varied from $\frac{1}{2}^{\circ}$ to 4° by means of a series of field stops.

Heating coils ran along the length of the photometer tube, which was well insulated thermally. The temperatures of the filter and photomultiplier compartments could be controlled independently by thermostats.

The photometer could be moved manually in both azimuth and zenith angles and locked in any required position. A sight mounted on one of the tubes allowed the photometer to be pointed at any desired auroral feature.

A Polaroid could be mounted on the front of each tube and rotated by a synchronous motor at 1 rev/min.

Indicators marked the recording chart every time the filter passed through the normal incidence position, or when the Polaroid maximum transmission direction passed through the vertical.

A standard light source was used for absolute calibration of each channel of the photometer. This consisted of a tungsten lamp whose current could be accurately controlled; the light from the lamp passed through two diffusing screens to give uniform illumination over the front of the photometer tube. A series of stops in the light source gave a 1:128 range of known intensities. Calibration of the light source was carried out by the National Standards Laboratory, CSIRO, before the expedition left Australia. The tungsten lamp could be replaced by a hydrogen lamp for wave-length calibration of the $H\beta$ filter.

The photomultiplier output was detected as individual pulses, which were amplified and fed to a rate meter. Tests with the standard light source showed that the system was linear in its response and gave best signal-to-noise ratio at an EHT voltage of 1700 V at the temperature of operation (0°C, thermostatically controlled).

(b) *Other Instruments*

Other instruments used in this investigation were:

- (1) Zenith photometer; 23° field of view, recording [OI] λ 5577 Å.
- (2) 27.6 Mc/s riometer (27° field of view) and 77 Mc/s riometer (13° field of view).
- (3) All-sky camera; one exposure per min.
- (4) Patrol spectrograph; one 45 and one 120 min exposure every 3 hr.
- (5) High dispersion spectrograph; dispersion 85 Å/mm.
- (6) H -component fluxgate magnetometer.
- (7) 5 kc/s v.l.f. recording equipment.
- (8) Cossor ionosonde.

(c) *Experimental Technique*

Throughout clear moonless nights, the $H\beta$ intensity was measured at 15° intervals along the auroral meridian (the perpendicular to the average direction of auroral arcs and corresponding closely to the eccentric dipole meridian). Each scan took about 25 min to complete (from 80° S. to 80° N.) and consisted of two filter tilting cycles at each point.

When quiet forms of visual auroras were present, their positions were noted and the $H\beta$ intensity was measured to the north, in, and to the south of the aurora, as well as at the normal scan positions. If a strong band of $H\beta$ was observed, its position was traced out in zenith and azimuth angles by further measurements.

When the onset of an auroral breakup event was observed (aurora in the northern sky becoming active), the photometer was fixed in either the magnetic or geographic zenith until the breakup was over, when routine scans were recommenced.

At times when the hydrogen emission was more or less uniform over the sky, scans were made perpendicular to the auroral meridian for van Rhijn height determination.

The polarization of the hydrogen emission was often examined by scanning the sky with the rotating Polaroid fitted to the front of the photometer.

III. DATA REDUCTION

(a) Derivation of $H\beta$ Intensity from the Photometer Records

(i) Filter Characteristics

The $H\beta$ multilayer interference filter used was 3 in. in diameter and, when received from the manufacturer, had a half-power bandwidth of 3.0 \AA and peak transmission of 28.5% at 4861.5 \AA at 20°C for normal incidence.

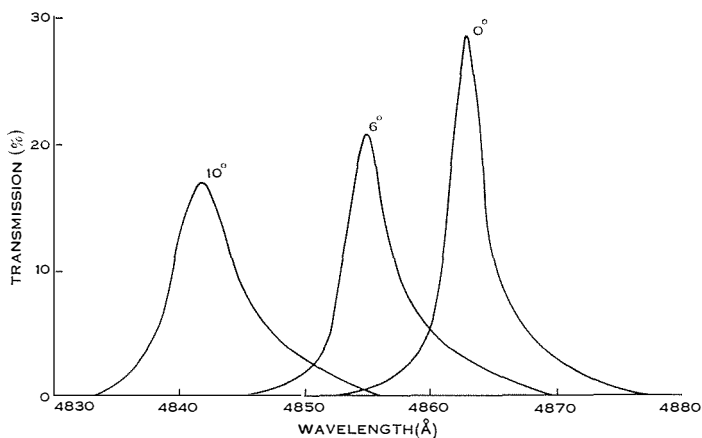


Fig. 2(a).—Filter transmission curves for angles of incidence 0° , 6° , and 10° .

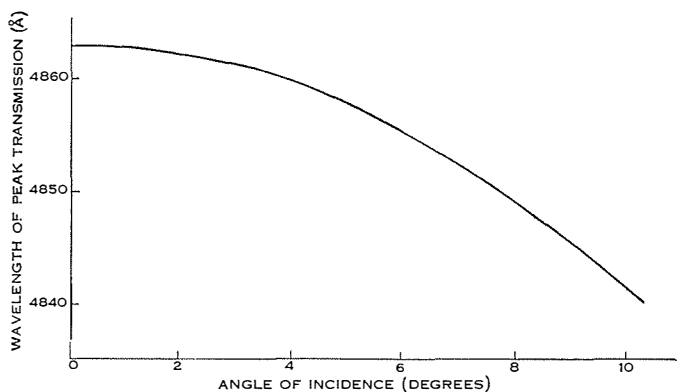


Fig. 2(b).—Wavelength of peak transmission of the filter at 20°C as a function of angle of incidence.

Filter transmission curves (as determined with a monochromator) for angles of incidence of 0° , 6° , and 10° are shown in Figure 2(a). Figure 2(b) shows the wavelength of peak transmission as a function of angle of incidence of the light. The wavelength of peak transmission increases with the temperature (for a given angle

of incidence) at $0.25 \text{ \AA}/\text{degC}$, while the bandwidth increases at $0.02 \text{ \AA}/\text{degC}$. As it was intended to scan the $H\beta$ line by tilting the filter, the filter was maintained at a temperature of 27°C to increase the wavelength of peak transmission to 4863 \AA . Unfortunately the wavelength of peak transmission decreased slowly with time (due to aging of the filter, perhaps accelerated by operation at elevated temperatures) and by the end of the auroral season a temperature of 65°C was required to keep the wavelength of peak transmission at 4863 \AA . At this temperature, the half-power bandwidth was 3.9 \AA . A monochromator was available at Mawson for regular checks on filter characteristics.

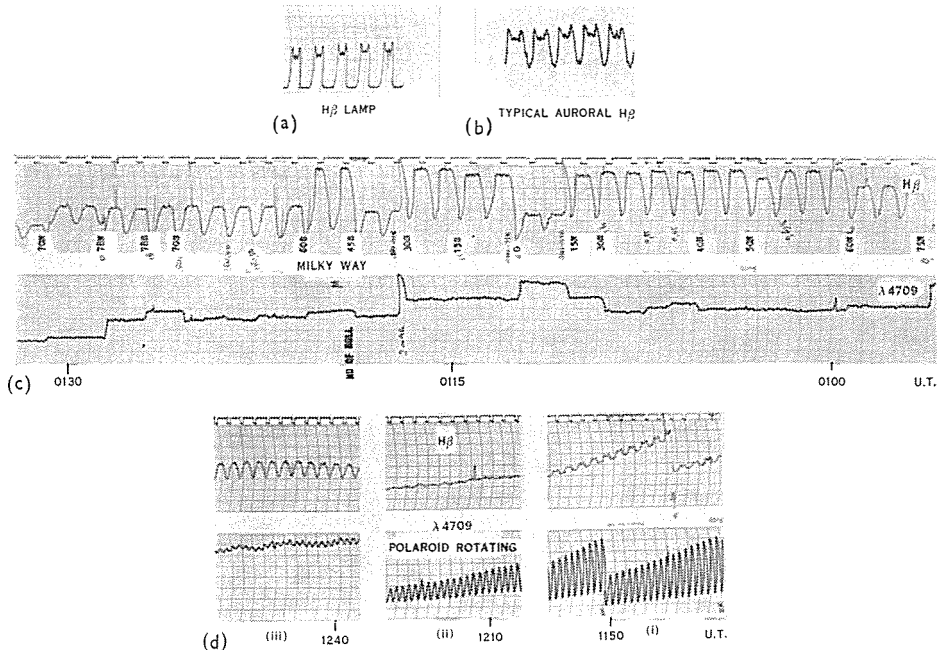


Fig. 3.—(a) Photometer trace obtained from a hydrogen spectral lamp. (b) Photometer trace obtained from auroral hydrogen emission. (c) Measurements of $H\beta$ intensity across the auroral meridian. The strong, narrow bandwidth, Milky Way signal is readily identifiable. (d) Measurement of $H\beta$ at various stages of sunset. The photometer is directed at the zenith and the polarization of the $\lambda 4709$ channel indicates the amount of scattered sunlight present. In (i) Fraunhofer absorption is evident; later, in (ii), auroral hydrogen emission cancels Fraunhofer absorption; in (iii) the auroral hydrogen emission is evident.

(ii) *Typical Profiles*

The trace obtained from the photometer viewing a hydrogen spectral lamp is shown in Figure 3(a). Note that the filter tilts from 0° to 10° and then back to 0° again in each cycle (of 1 min). The trace obtained from auroral hydrogen emission shows a much broader profile with the peak Doppler shifted towards shorter wavelengths to an extent depending on the direction of observation. A typical profile of auroral $H\beta$ is shown in Figure 3(b). The Doppler shift of the peak of the line profile can be obtained by measuring the distance between adjacent peaks on the

trace. A calibration curve, giving Doppler shift of the peak of the profile as a function of distance between recorded peaks on the trace, was determined using the monochromator, and is shown in Figure 4.

In interpreting the records, care must be taken that they are not contaminated by $H\beta$ from the Milky Way or by the scattered moonlight continuum, which includes $H\beta$ Fraunhofer absorption. The Milky Way contribution may be quite appreciable; intensities of 65 R being recorded. This contribution can be identified by the fact that

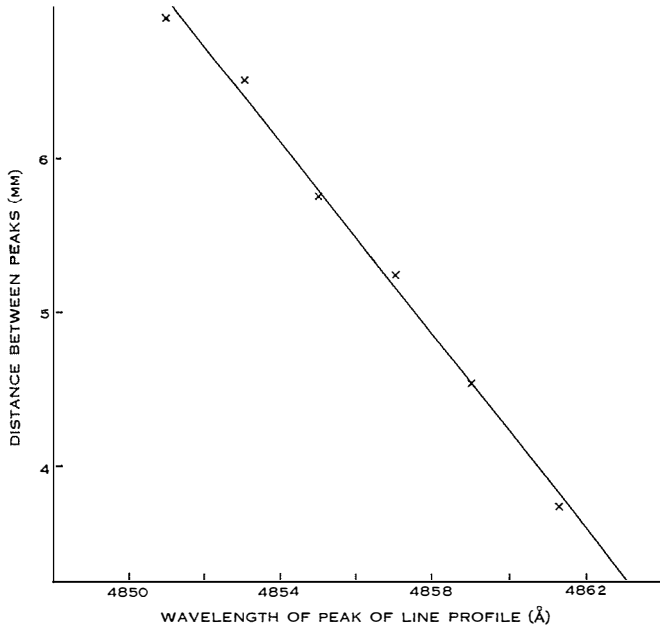


Fig. 4.—Calibration curve to determine Doppler shift of auroral hydrogen profiles from the separation of peaks on the photometer trace (chart speed 0.2 mm/sec).

the wavelength is unshifted and the profile much narrower than auroral $H\beta$. Lower-level Milky Way contamination, however, may pass undistinguished from auroral emission if the position of the Milky Way throughout observations is not noted. Figure 3(c) shows a scan across the sky in which the differences between auroral $H\beta$ and Milky Way $H\beta$ can be clearly seen.

The $H\beta$ Fraunhofer absorption in the continuous spectrum of scattered sunlight (at dawn and dusk) or of moonlight gives a trace of the form shown in Figure 3(d), and could at first be misinterpreted as Doppler shifted $H\beta$ emission. The “shift” as measured from the distance between peaks is far too high, however. In weak moonlight (for example, when the moon is just below the horizon) the Fraunhofer absorption is not so obvious and results in apparent reduction of the true auroral $H\beta$ signal.

Measurements of auroral $H\beta$ emission, then, cannot be made when the moon is above or just below the horizon, or if the Milky Way is in the field of view of the

photometer. The first of these conditions greatly reduces the number of nights on which observations may be made.

(iii) *Performance Characteristics of the H β Photometer*

Typical H β intensities were 25–50 R. It was found that a recording system time constant of 1 sec was required to give an acceptable standard deviation of the signal. H β intensities of 1 R could be measured under favourable conditions (steady background, no interference). Accuracy of Doppler shift measurements was $\pm 0.6 \text{ \AA}$. The minimum cycle time for tilting of the filter depended on the signal level and the acceptable standard deviation of the trace. Generally a cycle time of 1 min was used.

The accuracy of polarization measurements depended on the signal level, and was of the order of 10% for H β intensities of 10 R, and 2% for 50 R.

(iv) *Calculations*

The H β line was scanned by tilting the filter so that the wavelength of peak transmission moved to lower wavelengths. Tilting the filter from 0° to 10° allowed a wavelength scan from 4863 to 4841 \AA . The filter transmission curves were somewhat asymmetrical (Fig. 2(a)) and as the filter was tilted the transmission curves broadened and peak transmission decreased; at 10° the bandwidth was 5.5 \AA and the peak transmission 17%.

Because of the low intensity of the hydrogen emission, the maximum field of view of the photometer (4°) was used. This further complicated correction for filter transmission profile, as light passed through the filter over a range of incidence angles.

Effective transmission curves were computed as follows.

(1) Filter transmission curves $T(a, \lambda)$, where a is the tilt angle and λ the wavelength, were determined experimentally with parallel light and with values of a from 0° to 12° in steps of $\frac{1}{2}^\circ$ ($T(0, \lambda)$, $T(6, \lambda)$, and $T(10, \lambda)$ are shown in Fig. 2(a)).

(2) For a given tilt angle a and a field of view of 4° , light reaching the photomultiplier cathode makes angles of incidence with the filter between $|a-2|^\circ$ and $(a+2)^\circ$. This range was divided into $\frac{1}{2}^\circ$ intervals, that is, $|a-2|^\circ$ to $|a-1\frac{1}{2}|^\circ$, $|a-1\frac{1}{2}|^\circ$ to $|a-1|^\circ$, . . . $(a+1\frac{1}{2})^\circ$ to $(a+2)^\circ$.

Consider Figure 5, where the field of view is divided into a large number of elemental (square) areas; in practice, a 100 by 100 grid was used. Let P be the point $(1, (n_1/50)\tan 2, (n_2/50)\tan 2)$, where n_1 and n_2 are integers and $-50 \leq n_1, n_2 \leq 50$. Then ξ , as defined in Figure 5, is given by

$$\xi = \cos^{-1} \left[\frac{\cos a + (n_1/50)\sin a \tan 2}{[1 + \{(n_1^2 + n_2^2)/2500\}\tan^2 2]^{\frac{1}{2}}} \right].$$

ξ was calculated on an IBM 1620 computer for each of the points P, provided that $n_1^2 + n_2^2 \leq (50)^2$, and the results were divided into the eight divisions defined above. This gives the fraction of incident light that passes through the filter at angles of incidence defined by the limits of the above eight divisions. Call this fraction the

angle weighting factor $W(\alpha, \alpha + \frac{1}{2}n)$, where n takes integral values from -4 to $+3$, yielding eight angle weighting factors associated with each tilt angle α .

(3) The effective filter transmission curve for each tilt angle α is then given by

$$T_E(\alpha, \lambda) = \sum_{n=-4}^3 T(\alpha + \frac{1}{2}n, \lambda) W(\alpha, \alpha + \frac{1}{2}n).$$

Effective transmission curves were calculated on the IBM 1620 for $0^\circ \leq \alpha \leq 10^\circ$ in steps of 1° . The 4° field of view naturally results in a broadening of the filter transmission curves.

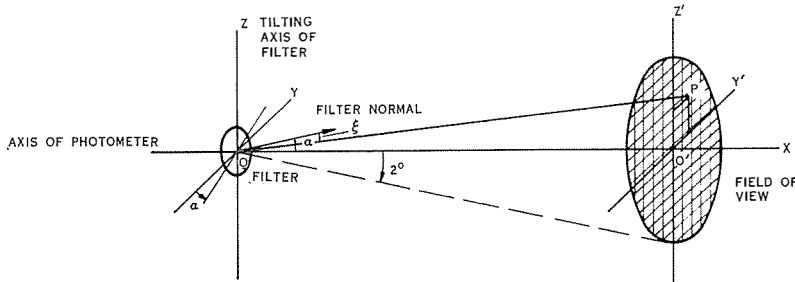


Fig. 5.—Geometry for the calculation of angle weighting factors $W(\alpha, \alpha + \frac{1}{2}n)$. $OO' =$ unit length, $\alpha =$ tilt angle, $\xi =$ angle of incidence of arbitrary ray $P-O$, and $2^\circ =$ field of view.

(4) The effect of the above considerations when measuring hydrogen line profiles with the photometer was then calculated. Experimental magnetic zenith and horizon profiles published by Zwick and Shepherd (1963), uncorrected for scattering, were used as “test” emission profiles and profiles for ϕ equal to 30° and 60° were obtained by interpolation (allowance being made for the cosine dependence of Doppler shift on ϕ). ϕ is here the angle between the line-of-sight and the magnetic field lines at the height of emission. Let the emission profiles be represented by the luminosity function $H(\phi, \lambda)$; the apparent profiles that would result if lines with these test profiles were scanned by the photometer were then calculated as follows.

For $0^\circ \leq \alpha \leq 10^\circ$ in steps of 1° , the expression

$$\int H(\phi, \lambda) T_E(\alpha, \lambda) d\lambda$$

was evaluated over the wavelength range of $T_E(\alpha, \lambda)$. The curve drawn through the 11 points so obtained gave the apparent profile as would be traced out by the scanning photometer as a function of α . This profile was converted to intensity as a function of λ using the $T_E(\alpha, \lambda)$ curves, the calculations again being performed numerically on an IBM 1620 computer.

As expected, the photometer and filter characteristics resulted in broadening of the test emission profiles and an overemphasis of the low wavelength portion of the profiles. The effects on Zwick and Shepherd’s horizon and zenith profiles are shown in Figure 6.

As a check, a “constant intensity profile”, that is, $H(\phi, \lambda) = \text{constant}$, was also examined. The apparent profile calculated showed a 6% modulation as the filter tilted from 0° to 10° and back again; this agreed with the modulation observed experimentally when the filter was tilted with a continuous light source (the standard light source) in front of the photometer.

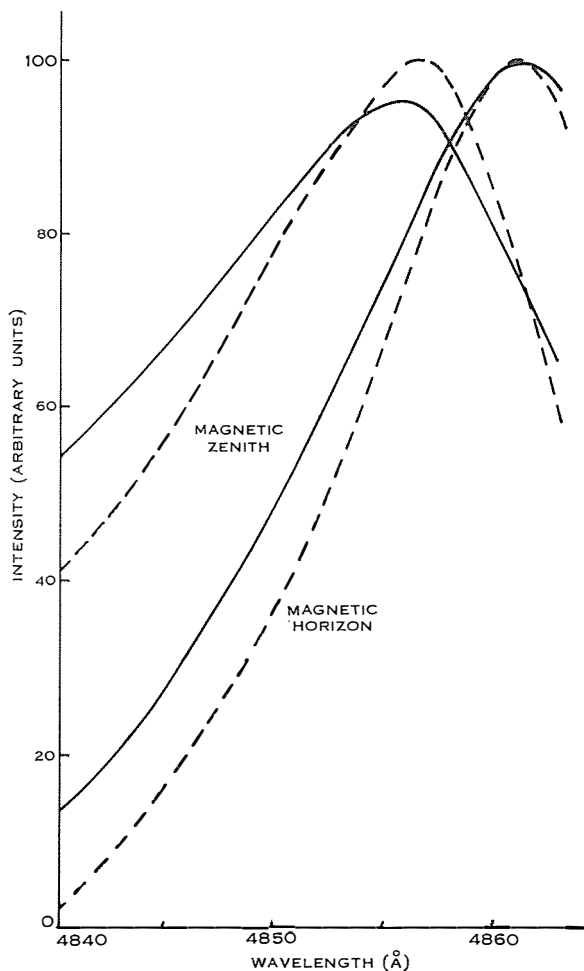


Fig. 6.—Effect of photometer and filter optics on Zwick and Shepherd's (1963) zenith and horizon profiles; dashed curves are the original profiles.

There is also a small effect of the filter and photometer optics on the measured Doppler shift of the peak of the line profile. They not only cause a broadening of the recorded profile but also a small change in the wavelength of the peak of the recorded profile. From Figure 6, the real Doppler shift is given approximately by

$$\Delta\lambda_{\text{real}} = \frac{7}{8} \times \Delta\lambda_{\text{measured}}.$$

(5) The $H\beta$ "intensity" I_{measured} is measured from the records as the difference of the maximum ($\alpha \simeq 3^\circ$) reading and the minimum ($\alpha = 10^\circ$) reading; that is, the modulation of the photometer output. $\alpha = 10^\circ$ corresponds to a wavelength of peak transmission of the effective profile of 4841 \AA . As can be seen from Figure 6, there is still an appreciable intensity of emission at 4841 \AA , increasing with Doppler shift. Thus as the Doppler shift increases, I_{measured} is, in fact, a decreasing fraction of the real intensity I_{real} . The ratio $I_{\text{real}}/I_{\text{measured}}$ is readily obtained from comparison of the calculated and test profiles (as in Fig. 6) and is shown plotted as a function of Doppler shift of the profile peak in Figure 7. This curve relates, of course, only to the assumed test profile.

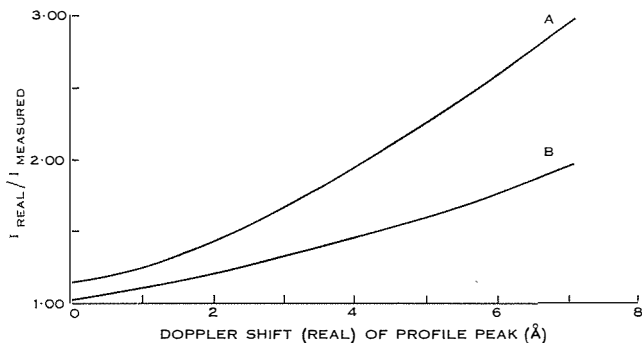


Fig. 7.—Variation of $I_{\text{real}}/I_{\text{measured}}$ with Doppler shift of the peak of the assumed line profile. A, Zwick and Shepherd's (1963) profiles; B, Veissberg's (1962) profiles.

Thus to obtain the real $H\beta$ intensity from the measured modulation of the photometer trace:

- (1) The Doppler shift in the magnetic zenith must be determined.
- (2) For each direction of observation, the angle ϕ between the line-of-sight and the magnetic field line at the height of emission must be calculated. This calculation must be carried out for the actual magnetic field configuration (not just for an assumed dipole field) and makes use of published magnetic declination and inclination charts (corrected to the year 1963.5). Calculations were made every 10° of zenith angle and every 20° of azimuth angle, for the assumed heights of emission. Because ϕ depends on the assumed height of emission and this is not known, all intensity calculations were carried out for two assumed heights of emission, 100 and 300 km. The Doppler shift is calculated from the $\cos \phi$ dependence.
- (3) From the Doppler shift in the direction of observation, I_{real} can be obtained using the graph of Figure 7.

It is important to note that the derived I_{real} also depends on the assumed test profile. Zwick and Shepherd's (1963) profiles discussed earlier were used. For most of this investigation, only relative intensities are important and these will not be greatly affected by the choice of test profile.

(v) *The Meaning of I_{real} for Auroral Hydrogen Profiles*

The above discussion has shown how I_{real} , defined as the peak height of the line profile, can be determined from I_{measured} , defined as the magnitude of modulation of the photometer trace. For a spectral line with no Doppler shift, the height of the line profile is proportional to the central intensity of the line, provided the line is symmetrical; this is not the case for Doppler shifted hydrogen lines.

Consider the source of radiation giving rise to the peaks of the horizon and zenith profiles, that is, the shaded areas of the profiles in Figure 8, where the width of the shaded area is small and equal for each profile.

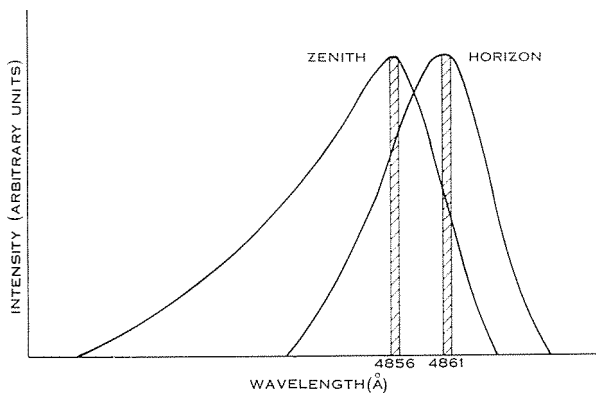


Fig. 8.—Arbitrary magnetic zenith and horizon line profiles—see discussion in Section III(•) (v).

For the zenith profile, the shaded area is due to radiation from hydrogen atoms moving along the lines of force (pitch angle zero) with a velocity corresponding to the Doppler shift of the peak, and also to radiation from hydrogen atoms with higher velocities but with finite pitch angles.

For the horizon profile, the shaded area is due to hydrogen atoms moving along a line of force with any value of velocity.

Thus to take I_{real} from emission in an arbitrary direction as a measure of the surface luminosity (photons $\text{cm}^{-2}\text{sec}^{-1}\text{sr}^{-1}$) in that direction would be quite erroneous. The only meaningful measure of the surface luminosity when emission lines are subject to variable Doppler shift is the integrated intensity $\int I_{\lambda} d\lambda$ over the width of the line. This will be a valid measure of surface luminosity, or of emission rate (photons $\text{cm}^{-2}\text{sec}^{-1}\text{column}^{-1}$), if hydrogen radiation is isotropic, which seems to be a reasonable assumption (Chamberlain 1961).

(vi) *Derivation of the Integrated Intensity*

The areas under Zwick and Shepherd's (1963) zenith and horizon profiles, and the test profiles interpolated between them, were measured and factors ($F(\eta)$) relating profile peak height and area were derived. $F(\eta)$ was defined to satisfy

$$F(\eta) I_{\text{real}}(\eta) = I_{\text{real}}(0)$$

for profiles from observation angles $\eta = 0^\circ, 30^\circ, 60^\circ,$ and 90° from the magnetic zenith, and of equal area. $F(\eta)$ varied from 1.00 for the magnetic zenith direction to 1.53 for the magnetic horizon direction. Note that $F(\eta)$ depends on the assumed height of emission; all calculations were carried out for the two assumed heights of emission, 100 and 300 km, mentioned previously.

(vii) *Conclusion*

All measurements of the modulation of the photometer trace were converted (on an IBM 1620 computer) to integrated intensities following the procedure set out above, and for the two assumed heights of emission.

When scans across the meridian were being considered, the integrated intensities were calculated and plotted directly as functions of latitude by a CDC 3200 computer. The latitude of emission for a given zenith angle of observation depends, of course, on the assumed height of emission. Again, all calculation and plotting was carried out for the two assumed heights of 100 and 300 km.

From this point in the present paper, whenever the intensity of hydrogen emission is mentioned, all the above computations are implied to have been performed and it is the resulting integrated intensity that is being referred to.

IV. NATURE OF THE HYDROGEN EMISSION

(a) *Absolute Intensity of the Hydrogen Emission*

Regular calibration of the $H\beta$ photometer with the standard light source permitted conversion of the photometer readings to absolute radiation intensity. Typical values of the peak $H\beta$ intensity during the night were 25–50 R (corrected “to the zenith” for the van Rhijn effect). The maximum value of $H\beta$ intensity recorded during the year was 150 R. As a further check, the maximum $H\beta$ intensity from the Milky Way was measured (65 R averaged over the 4° field of view of the photometer) and compared with the value calculated from published Milky Way $H\alpha$ isophotes (Johnson 1960) assuming a Balmer decrement of 3.0; the agreement was satisfactory.

The $H\beta$ intensities measured at Mawson are only 10–20% of published northern hemisphere values; this is thought to be due to an important sunspot cycle effect on hydrogen emission intensities (Eather and Sandford 1966). Most of the observations from the northern hemisphere were made around the period of maximum sunspot activity.

(b) *Doppler Shift*

The distance between peaks on the recorded trace allows the measurement of the Doppler shift of the $H\beta$ emission (Fig. 4). The accuracy of measurement was estimated at $\pm 0.6 \text{ \AA}$, the main error arising in the exact location of the peaks, as these peaks were rather broad (see Fig. 3).

Measured Doppler shifts of the $H\beta$ line varied from 5 to 7 \AA in the magnetic zenith direction; the Doppler shift on a particular night could vary by $\pm 1 \text{ \AA}$, but this may merely reflect inaccuracies of measurements. Doppler shifts, plotted against

angle between the line-of-sight and the magnetic field lines at 100 km, are shown in Figure 9 at three different times on the one night. The expected cosine dependence on the angle between the direction of observation and the magnetic field lines is well verified. Note that the measured Doppler shift has fallen below the cosine curve towards the end of the first scan, suggesting that the shift had decreased during the scan. This agrees with the lower shift recorded in the magnetic zenith during the scan. This agrees with the lower shift recorded in the magnetic zenith during the scan.

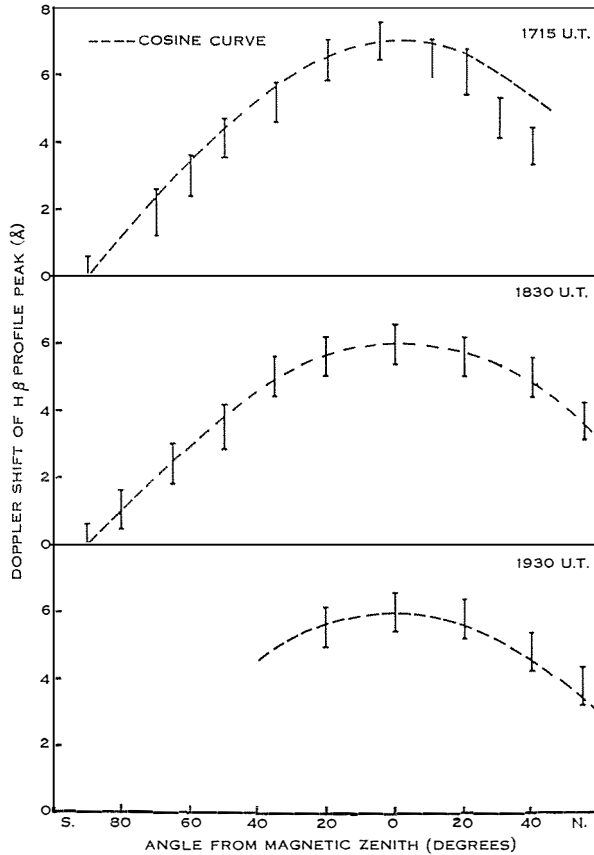


Fig. 9.—Doppler shift of auroral hydrogen line profiles as a function of the angle between the line-of-sight and the magnetic field at 100 km, at three different times on the night of September 13, 1963.

the second scan. These differences between maximum Doppler shifts are little larger than the estimated accuracy of measurement and no attempt was made to relate the apparent changes in shift to other variables such as intensity, magnetic activity, or phase of the auroral display. The safe conclusion is that the Doppler shift remains fairly constant at $6 \pm 1 \text{ \AA}$ (for $H\beta$) over a wide range of conditions of line intensity, auroral and magnetic activity. This shift corresponds to a velocity of $370 \pm 60 \text{ km/sec}$.

No systematic attempt was made to measure line widths, as such measurements are very susceptible to uncertainties in the background level. A few random measurements on records showing strong $H\beta$ indicated half intensity line widths of 15 to 20 Å, similar to those reported by other workers (Johansen and Omholt 1963).

Plate 1 shows some auroral spectra taken with the high dispersion and patrol spectrographs; the first spectrum shows the Doppler shift of the $H\beta$ line in the magnetic zenith direction, while the second spectrum shows the unshifted $H\beta$ line from the magnetic horizon direction.

(c) *Narrow Profiles*

There have been reports of narrow hydrogen lines recorded in the auroral zone (Montalbetti 1959; Prokudina 1959; Malville 1960; Herman and Belon 1961). No narrow auroral hydrogen line profiles were observed during the year's observations at Mawson. Hydrogen radiation from the Milky Way exhibits a narrow profile, which is readily identifiable in the stronger regions of the Milky Way but could easily be mistaken for auroral hydrogen emission in the weaker parts of the Milky Way field. In particular, if long spectrographic exposures are made, care must be taken that the Milky Way does not pass through the field of view during the course of observations.

(d) *Polarization*

Ginzburg (1943) drew attention to the possibility that permitted auroral radiation might be polarized, owing to ordered motion of the exciting particles.

Polarization measurements were made on the $H\beta$ line by fitting the rotating Polaroid to the front of the photometer tube and searching for polarization at the peak position of the profile (filter stationary at maximum transmission) and then of the background (filter stopped at 10°). For strong auroral $H\beta$ (~ 50 R) it was estimated that a polarization of 2% could have been detected, but for weak $H\beta$ (~ 10 R) the polarization would have had to be of the order of 10% to be detected.

No polarization of the $H\beta$ radiation was detected at any time. It is evident then that scattering of auroral hydrogen radiation from one region of the sky to another is unimportant, although many investigators have assumed large atmospheric scattering corrections in explaining observed shapes of hydrogen line profiles. This will be discussed in more detail in Section VI(e).

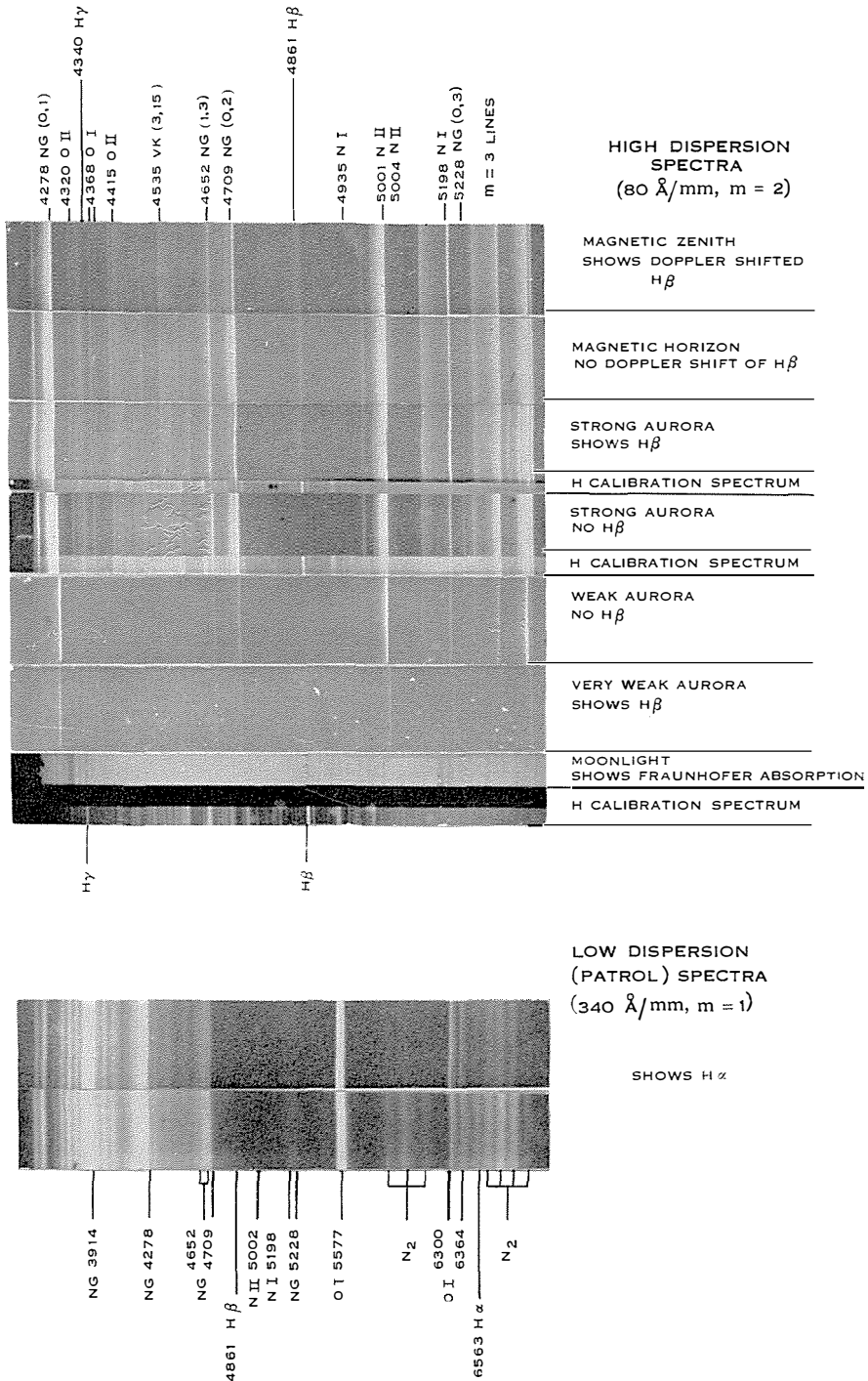
The $\lambda 4709$ and $\lambda 6300$ emissions were also examined for polarization on occasions; again no polarization was detected, in agreement with the findings of other workers (Bricard and Kastler 1947, 1948, 1950). Polarization of the order of 2% would have been detectable for these emissions.

V. RELATION TO OTHER AURORAL PHENOMENA

(a) *Relation of the Hydrogen Emission to Other Emissions*

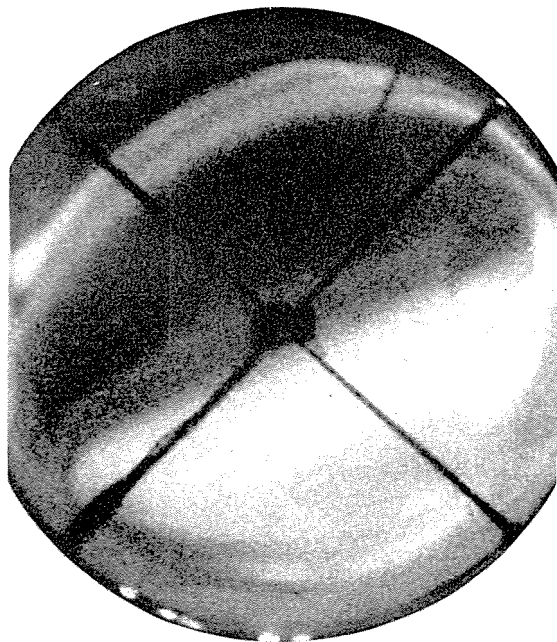
The second channel of the photometer was used to monitor either the $N_{\frac{1}{2}}^+$ $\lambda 4709$ band or the [OI] $\lambda 6300$ line. The $\lambda 4709$ band is representative of allowed transitions after high energy electron excitation, while the $\lambda 6300$ line is usually considered to be associated with high, red, type A aurora, and to be due to excitation

AURORAL HYDROGEN EMISSION



Some auroral spectra recorded at Mawson during 1963.

AURORAL HYDROGEN EMISSION



All-sky photograph showing strong aurora covering the northern sky at Mawson. It may be seen there there is little light scattered to the southern sky.

by lower energy electrons. A number of workers have reported correlation between hydrogen emission and the red $\lambda 6300$ line (Vegard 1955; Galperin 1959).

On no occasion during the year's observations did the hydrogen line intensity show a dependence on the intensity of $\lambda 4709$ or $\lambda 6300$ associated with visual auroras, which are presumed to be excited by electron bombardment. An example of lack of correlation of $H\beta$ and $\lambda 4709$ is shown in Figure 10(a). However, when hydrogen emissions were observed without visual auroras, the variations in $H\beta$ intensity sometimes correlated well with the variations in $\lambda 4709$ intensity, as illustrated in Figure 10(b). This suggests that the variations in $\lambda 4709$ in such cases are excited by proton bombardment.

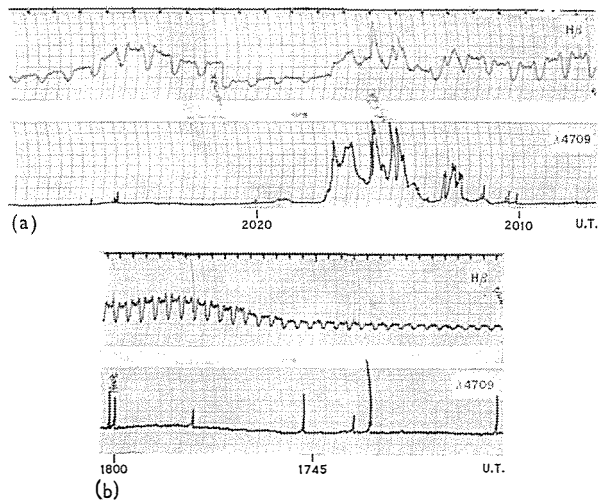


Fig. 10.—(a) Illustrating absence of correlation of $H\beta$ with $\lambda 4709$ (rayed bands in field of view). (b) Example of a large and unusually rapid change in $H\beta$ intensity associated with a change of similar form in $\lambda 4709$ intensity, suggesting that the latter was due to proton precipitation. No visible aurora was present.

The character of hydrogen intensity fluctuations (when observed) was in general very different from those of $\lambda 4709$ and $\lambda 6300$. The hydrogen emission was much steadier than the visual emissions, where the intensity could change by orders of magnitude in periods of seconds. No such behaviour was ever exhibited by the hydrogen emission, in which intensity fluctuations typically took place over periods of tens of minutes and the magnitude of fluctuations never exceeded 200%. Such changes could have been due to overall movements of the zone of emission rather than to absolute changes in hydrogen intensity.

(b) Relation to Visual Auroral Forms

When quiet auroral forms were present, the $H\beta$ intensity was measured south, in, and to the north of the forms. Similar measurements were made on active forms that were reasonably stable in position. When the aurora became very active, the photometer was left in a fixed position and detailed visual observations were made to determine the type of aurora in the field of view.

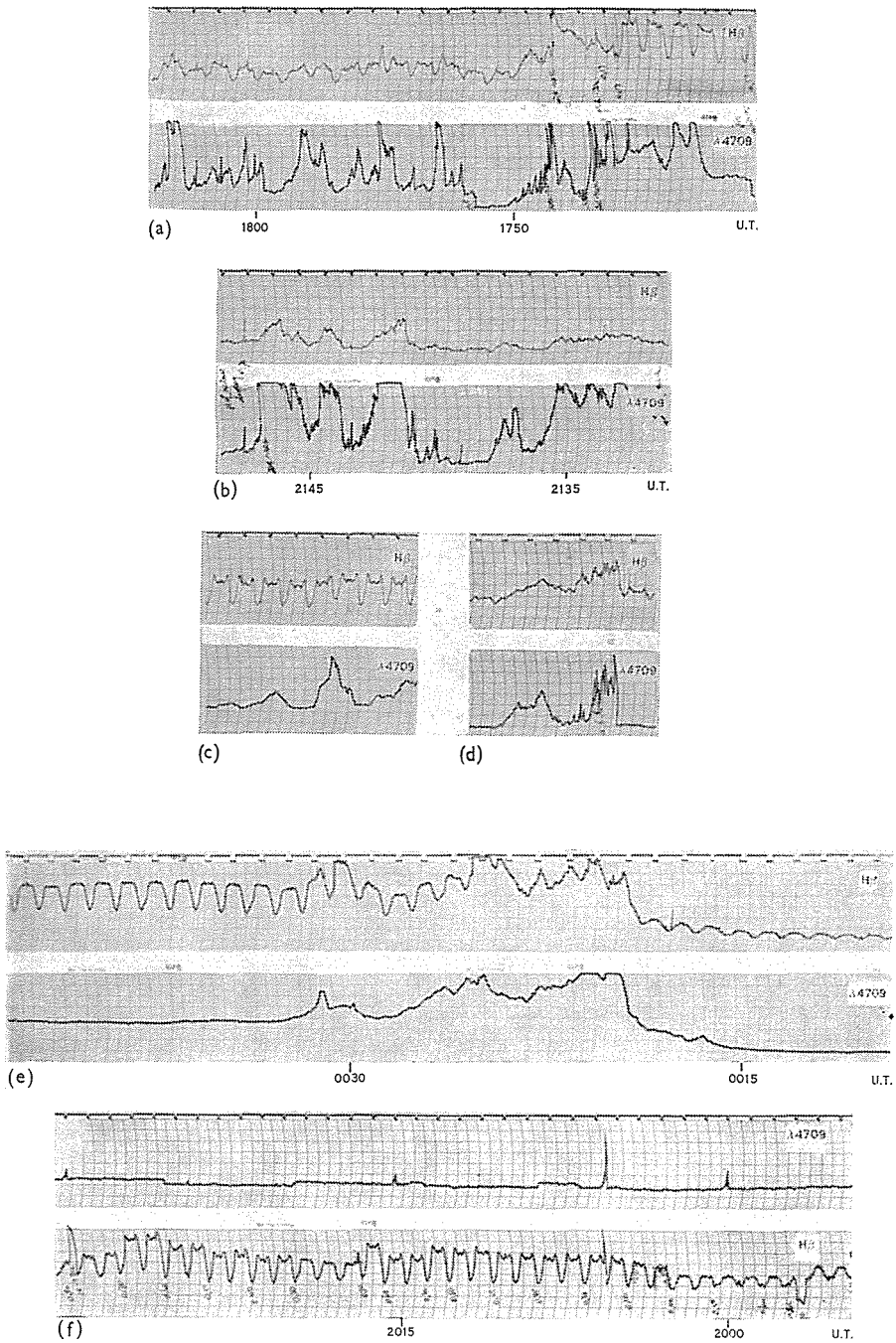


Fig. 11.—(a) Hydrogen emission present with active visual aurora. (b) Active visual aurora with no hydrogen emission. (c) Quiet auroral band with hydrogen emission. (d) Active rayed band with no hydrogen emission. (e) Hydrogen emission in a quiet auroral arc. (f) Strong hydrogen emission with no visual aurora.

Hydrogen emission was observed in all auroral forms at some time during the year and, similarly, all auroral forms were observed at some time without any hydrogen emission. Some examples of records obtained are shown in Figures 11(*a*) to 11(*f*). Hydrogen emission was usually present in some part of the sky during the night, and thus was frequently present in the absence of visual aurora (see Fig. 11(*f*)). Whether or not hydrogen radiation was observed in a visual form depended simply on the relative locations of the form and the hydrogen emission zone. This zone was typically a wide ($\gtrsim 5^\circ$ of latitude) steadily emitting region upon which discrete fluctuating visual auroras could be superimposed. In all cases, however, (except during a disturbed period at the auroral breakup) the maximum of the hydrogen emission zone was situated north of the northernmost visual aurora (that is, equatorwards). Typical examples of this are shown in Figure 12.

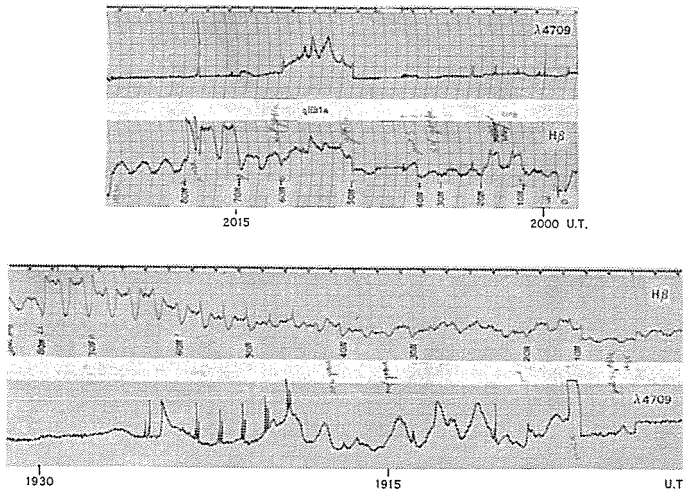


Fig. 12.—Examples of the maximum of the hydrogen emission zone situated north of the northernmost visual aurora.

In many cases there was an apparent enhancement of hydrogen emission in visual auroras near the northern horizon, although enhancements were not observed in similar displays when they were located near the zenith. This apparent enhancement is due to a combination of the van Rhijn effect and atmospheric extinction. For a uniformly emitting layer, the van Rhijn effect results in an increase (by a factor of approximately two, depending on height of emission) in the recorded signal at zenith angles of 70° – 75° , compared with the signal at the zenith (see Section VI(*a*) for a discussion of the van Rhijn effect). At higher zenith angles, atmospheric extinction causes a fall in the recorded intensity. Thus for a uniform emitting layer, the measured intensity as a function of zenith angle is as shown in Figure 13 (see also Fig. 15). Scanning through hydrogen emission near the horizon, then, will result in an enhanced $H\beta$ signal at about 75° , even though the actual emission may be uniformly distributed over the sky. Further enhancement results if the hydrogen emission zone has a maximum to the north of the visual aurora, as always appears to be so.

There was only one auroral type in which hydrogen emission was recorded on almost (but not all) occasions; this was the diffuse glow. This observation will be discussed in the next section.

The $H\beta$ intensity on a particular night was not correlated with visual auroral activity or intensity. A faint aurora could accompany long intense hydrogen emission, or strong aurora could occur with only faint hydrogen emission.

The auroral spectra shown in Plate 1 illustrate some of the points discussed in the above two sections.

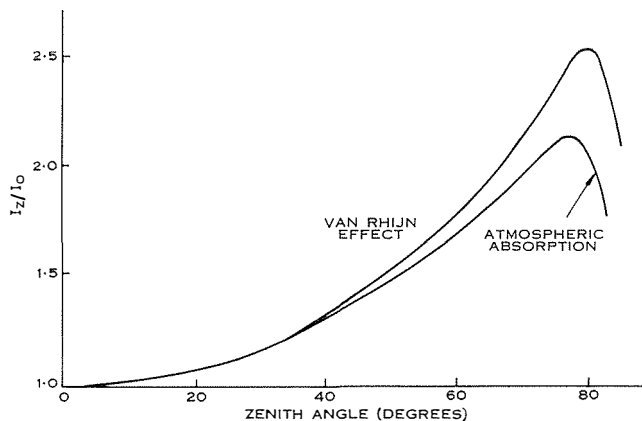


Fig. 13.—Ratio of intensity measured at a given zenith angle to that measured in the zenith, for an assumed thin uniformly emitting layer at the indicated height. A combination of the van Rhijn effect and atmospheric extinction results in an apparent band of emission with a maximum intensity at a zenith angle of about 75° .

(c) Relation to the Auroral Breakup Event

During the hour or so before the auroral breakup event the $H\beta$ intensity gradually decreased to a low level, often zero, in the zenith and to the south. There was still appreciable emission to the north on such occasions. This suggests that the fall in intensity was a result of the zone moving north of the station rather than of an overall decrease in the brightness of the emitting region.

During and after the breakup event, the $H\beta$ intensity usually increased over the whole sky. The intensity at this stage was of the same order as, or perhaps less than, that observed when the hydrogen emission was present over the sky earlier in the night; it was never significantly greater than that observed earlier in the night. Figures 14(a), 14(b), and 14(c) are typical of the behaviour described.

The hydrogen emission at this stage seemed to be associated with the diffuse patchy luminescence that usually covered the sky after the auroral breakup. Scans across the sky during such periods showed, however, that although the visual radiation was patchy spatially the hydrogen radiation was uniformly distributed. It is thus thought that the correlation reported (Yevlashin 1961, and others) between hydrogen emission and auroral glow is really a correlation with the breakup event

(as diffuse glows invariably occur after breakup), rather than a correlation with the diffuse glow as a distinct auroral form. This is supported by the observation that, whereas diffuse auroras were often present even an hour after the auroral breakup, hydrogen emission over the sky had always disappeared by then and was again only present in the northern sky. Also, auroral breakup events that were not accompanied by detectably enhanced hydrogen emission, yet were still accompanied by post-breakup auroral glow, often occurred.

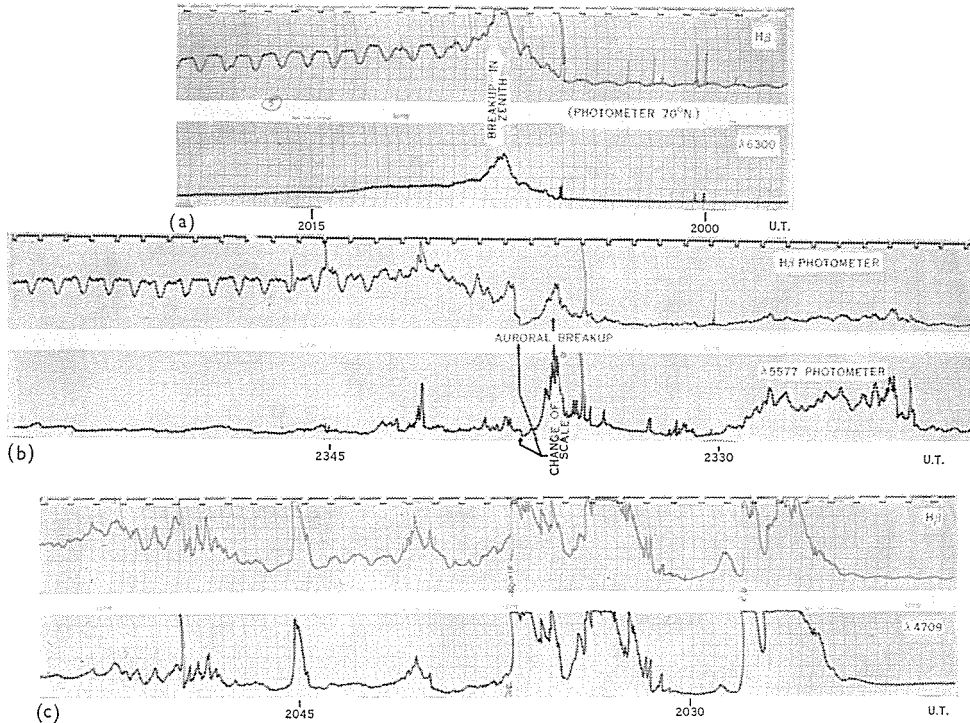


Fig. 14.—(a) Increase in $H\beta$ intensity 70° N. after an auroral breakup event in the zenith. (b) Increase in zenith $H\beta$ intensity after an auroral breakup event. (c) Example of a strong breakup event with only a small (but detectable) increase in $H\beta$ over the sky.

(d) Diurnal Latitude Movements of the Hydrogen Emission Zone

During the winter months, observations were usually made between 1400 and 0200 U.T. (local midnight at Mawson is at 2000 U.T.). The following results relate to movements of the zone within this period (during autumn and spring only part of the overall behaviour could be observed). All measurements were first corrected for the van Rhijn effect, for the assumed heights of emission of 100 and 300 km. The assumed height of emission did not affect any conclusions regarding latitude movements of the zone.

Early in the night, the maximum of the hydrogen emission was situated south (that is, polewards) of the station, usually near the horizon (see Fig. 15). The zone

then moved gradually northwards and the maximum was situated in the zenith at about 1500–1700 U.T. When the maximum of the zone was located in the zenith, hydrogen emission was usually recorded over the whole sky, indicating that the “half-intensity bandwidth” of the zone was of the order of (or greater than) 7° of latitude (for an assumed height of emission of 100 km). Thus when the maximum of the zone was near the northern horizon, there should still have been an appreciable emission from the zenith. The narrowest band of hydrogen emission observed was about 3° of latitude, for an assumed height of emission of 100 km.

The maximum of the emission zone had normally reached the region of the northern horizon by 1900 U.T. On some nights the intensity in the north then gradually decreased, suggesting that the zone had moved further north; on other nights the intensity in the north and zenith remained fairly constant, suggesting that the northern limit of the hydrogen zone movement corresponded to the latitude of the northern horizon at Mawson.

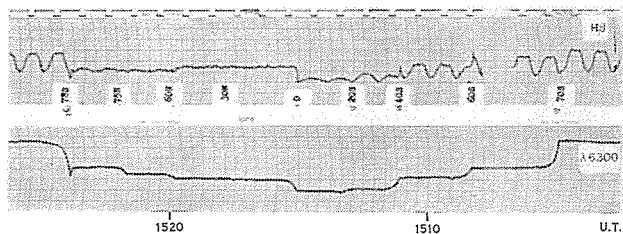


Fig. 15.—Example of hydrogen emission zone situated south of Mawson early in the night. It is also interesting to note the variation in λ 6300 intensity across the meridian (the van Rhijn effect is quite evident).

The movement of the hydrogen emission zone from south to north always preceded the movement of the visual aurora from south to north. (As mentioned earlier, the maximum of the hydrogen emission zone was always located north of the northernmost visual aurora.) Quiet visual arcs and bands typically appeared south about 1500 U.T. and gradually moved northwards over a period of about 3 hr. The movement of the visual zone northwards was often not a steady progression (as was that of the hydrogen emission zone) and a number of southward recessions could be superimposed on the general northward movement.

An example of the behaviour discussed is shown in Figure 16, where the $H\beta$ intensity along the auroral meridian is shown plotted at regular intervals during the night.

Once the hydrogen emission zone had reached its furthest northern excursion, the visual zone approached it and the two finally merged; this normally occurred about magnetic midnight, or a little later. It may be significant that it was not until after the zones merged that the auroral breakup event occurred, as if in some way the merging initiated the event.

As discussed previously (Section (c) above) the hydrogen emission zone spread and covered the sky during and after the auroral breakup event (as did the visual

aurora). Breakup usually occurred between 2000 and 2200 U.T. The hydrogen emission intensity then steadily decreased over the sky; within about half an hour the maximum of the zone was back near the northern horizon and there was no hydrogen emission from the south. The visual aurora at this stage consisted of sporadically active forms over the sky, usually tending to be confined to the south. This stage of the nightly behaviour was usually reached by 2100–2300 U.T.

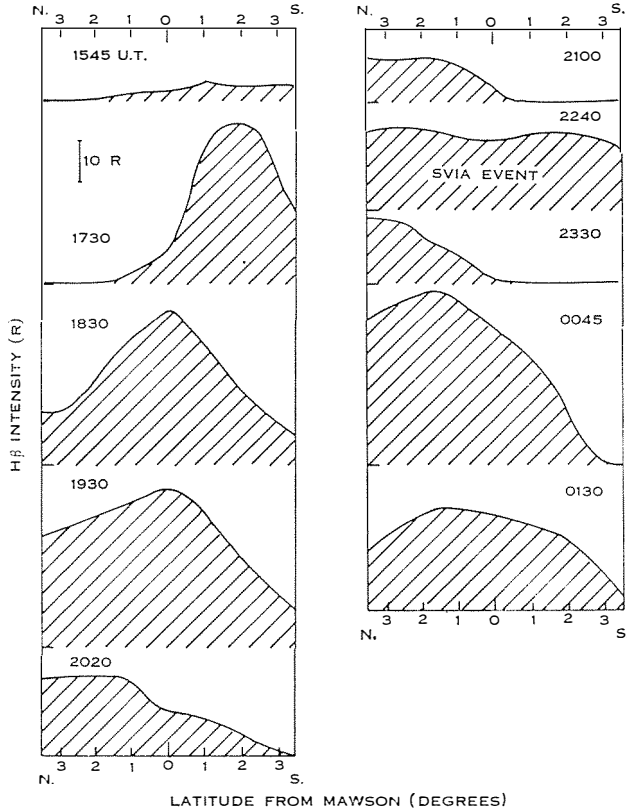


Fig. 16.— $H\beta$ intensity across the auroral meridian, plotted (at times shown) throughout the night of August 14, 1963, against degrees of latitude from Mawson for an assumed height of emission of 100 km.

On some nights the maximum of the hydrogen emission zone remained to the north (after the auroral breakup) with moderate intensity until dawn. On other nights the intensity decreased to zero while the zone was still located to the north. On a few nights the zone had started to return southward before sunrise, and the southward movement could at times be traced until the maximum was located overhead or to the south, before twilight stopped observations. Visual auroras had usually disappeared to the south before dawn.

During autumn and spring, the hydrogen emission zone was already to the north when the end of twilight allowed observations to be commenced, and was still to the north when morning twilight stopped observations.

The extent of the latitude drift of the hydrogen emission zone is of the order of the horizon-to-horizon distance at an assumed height of say 100 km (where "horizon" refers to a zenith angle of about 80°), corresponding to about 10° of latitude. The drift may have been larger on nights when the hydrogen emission appeared to move over the northern horizon, but, as hydrogen emission could still be observed at the horizon, the maximum was probably no more than 3° beyond the horizon.

(e) *Hydrogen Emission and V.L.F. Radiation*

A number of proton processes have been proposed as mechanisms for the excitation of v.l.f. radiation. Proton cyclotron radiation could give rise to v.l.f. emissions up to 800 c/s, and relativistic protons could give rise to synchrotron radiation at higher frequencies. However, there are probably not enough relativistic protons to account for observable intensities (Dowden 1963). Plasma oscillations and Doppler shifted proton cyclotron radiation have also been suggested as possible mechanisms whereby incoming protons could produce v.l.f. radiation.

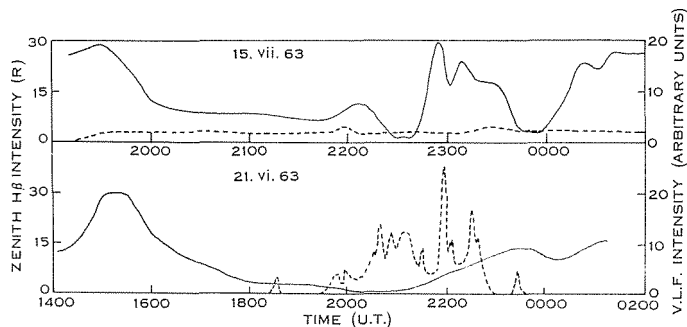


Fig. 17.—Zenith $H\beta$ intensity and 5 kc/s v.l.f. radiation throughout two nights. — $H\beta$ intensity; - - - v.l.f. intensity.

If incoming protons are important in generating v.l.f. radiation in the auroral zones and if they also result in hydrogen emission, then the v.l.f. intensity should be related to the hydrogen emission intensity in the zenith; that is, whenever strong $H\beta$ radiation was recorded in the zenith, v.l.f. radiation should also have been recorded (but not necessarily vice versa, as v.l.f. radiation, although it may penetrate through the ionosphere from above only through a very small allowed cone of incidence angles, may spread out below the ionosphere and propagate great distances within the earth-ionosphere wave guide—see Helliwell 1962).

Figure 17 shows $H\beta$ intensity in the zenith plotted against the level of 5 kc/s v.l.f. radiation on two different nights; there is obviously no correlation between the two phenomena. This does not exclude the possibility that v.l.f. radiation at 800 c/s could be related to hydrogen emission.

(f) *Association of Hydrogen Emission with E_s Ionization*

In this section, three types of E_s ionization, namely, "r" type, "a" type, and "f" type will be discussed. Briefly, the difference between r type and a and f type

E_s is that r type is non-blanketing and shows an increase in virtual height at the high frequency end similar to group retardation, whereas a and f types are blanketing and show no group retardation.

Figure 18(a) shows the average percentage hourly occurrence for the year of the different types of E_s found at Mawson (Schaeffer, personal communication). r type is the most common type observed, so that some caution must be exercised in assuming a causal relation with hydrogen emission from simple occurrence correlation. Figure 18(b) is a similar plot, except that only strong E_s layers, reflecting to at least 5 Mc/s, are included.

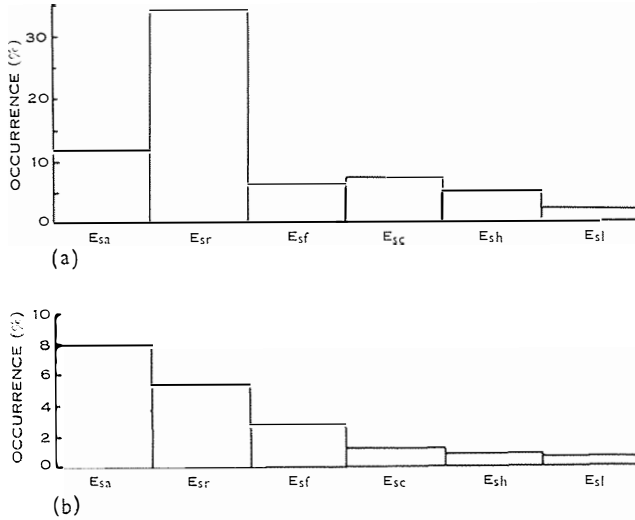


Fig. 18.—(a) Histogram showing the percentage occurrence distribution of the different types of E_s observed at Mawson. (b) Histogram showing the percentage occurrence distribution of the different types of E_s with $f_o E_s \geq 5$ Mc/s.

The observational technique of continually scanning the sky with the photometer did not allow a statistical analysis of the diurnal behaviour of hydrogen emission in the zenith. However, from the earlier descriptions of diurnal latitude movements of the hydrogen emission zone (Section (d) above), the characteristic diurnal variation of zenith hydrogen emission may be summarized: little emission before 1400 U.T.; a peak of emission between 1500 and 1700 U.T. as the zone passes overhead, moving equatorward; a minimum around 1900 U.T. when the zone is north of Mawson; a second maximum around 2000–2200 U.T. associated with the spreading of hydrogen emission across the sky during and after the auroral breakup; a second minimum as the hydrogen emission zone withdraws to the north again; finally another maximum if the hydrogen emission zone passed overhead again around or after 0200 U.T. whilst moving back to the south.

Figure 19(a) shows the diurnal curves for the percentage hourly occurrence of the different types of E_s at Mawson during 1963 (Schaeffer, personal communication). r type E_s shows a very similar diurnal behaviour to that described for the

hydrogen emission, exhibiting three definite peaks at times close to those of maximum zenith hydrogen emission. Both a and f types show only one peak around local midnight. Figure 19(b) shows similar diurnal curves for strong E_s layers ($f_o E_s \geq 5$ Mc/s); note that the peak of r type E_s occurrence at 2200 U.T. is here the principal occurrence maximum, whereas it is the smallest of the three occurrence maxima when all r type E_s events are included. This suggests that the hydrogen emission associated with the auroral breakup is also associated with "stronger" r type E_s ionization. The importance of this point has been discussed in detail by Eather and Jacka (1966).

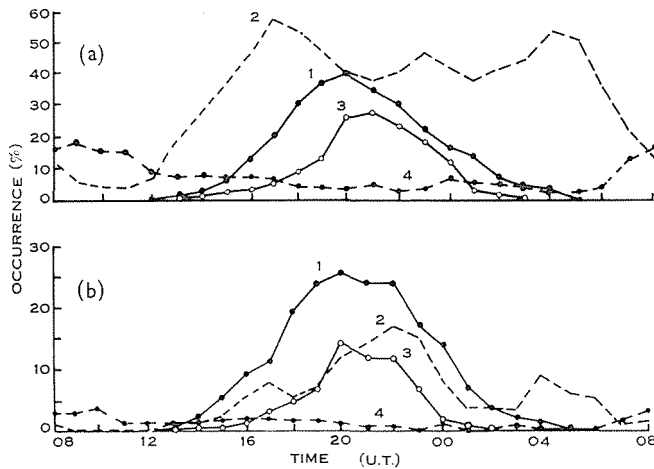


Fig. 19.—(a) Diurnal variation curves of percentage hourly occurrence of the different types of E_s . (b) Diurnal variation curves of percentage hourly occurrence of the different types of E_s with $f_o E_s \geq 5$ Mc/s. 1, E_{sa} ; 2, E_{sv} ; 3, E_{sr} ; 4, E_{so} .

Thus there appears to be a definite correlation between the occurrence of r type E_s ionization and the occurrence of hydrogen emission in the zenith. a and f type E_s , on the other hand, seem to be associated with visual auroras; this is indicated by the following behaviour of the percentage occurrence curves.

- (1) The percentage occurrence of a and f types begins to rise well after the percentage occurrence of r type begins to rise; similarly, the visual aurora moves from south to north some time after the movement of the hydrogen emission zone from south to north (Section (d)).
- (2) The peak of a and f type occurrence, between 1900 and 2200 U.T., covers the period in which the visual aurora passes overhead, moving northward, and also the period of the breakup event. The irregular spatial movements of visual auroras and associated E_s ionization have resulted statistically in a broad single occurrence maximum. As mentioned before, the northward progression of the visual aurora is far from regular, often including southward recessions superimposed on the general northward movement.

- (3) The percentage occurrence of a and f types falls off much earlier than that of r type; similarly, visual auroras usually disappear to the south after the breakup, whereas hydrogen emission withdraws to the north and returns southwards several hours later.

It also seemed desirable to examine minute-to-minute changes in the intensity of zenith hydrogen emission for correlation with the occurrence of the various types of E_s . Only a few records of nights where the photometer had been stationary in the zenith all night, providing continuous records of $H\beta$ zenith intensity, were available. Figure 20 shows two examples of zenith $H\beta$ intensity throughout the night,

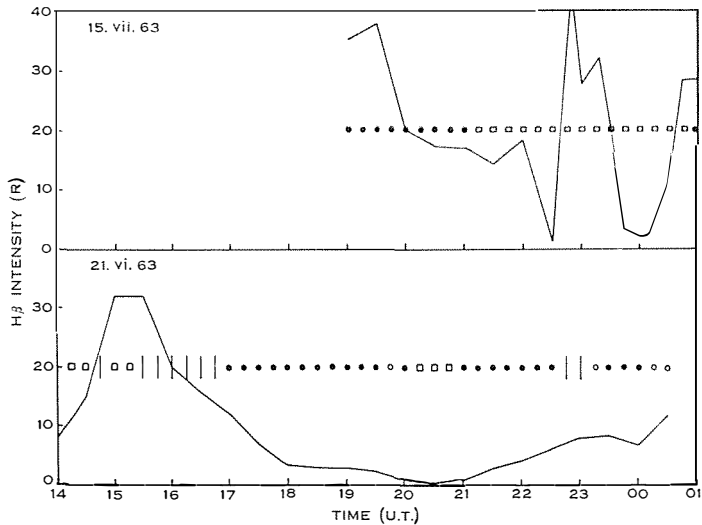


Fig. 20.—Zenith $H\beta$ intensity plotted throughout two nights, together with the occurrence and type of E_s ionization. | Blackout; \square E_{sf} ; \bullet E_{sr} ; \circ E_{sa} .

plotted together with the occurrence of the various types of E_s in the zenith. At first inspection, the correlation between hydrogen emission and r type E_s does not appear to be very good; however, if it is assumed that the presence of a or f type E_s precludes the observation of r type, then the correlation is good. Whether this is a valid assumption is not known, but it does not seem unreasonable that the onset of electron precipitation (causing visual auroras and a and/or f type E_s) could give rise to E_{sa} or E_{sr} layers at lower heights than the E_{sr} layer. The E_{sa} and E_{sr} layers are usually considered to be blanketing and could prevent observations of the increase in virtual height with frequency associated with E_{sr} . Correlations may also fail to appear from records of individual nights because of the frequent difficulty of identifying transitions between different types of E_s ionization. Diurnal averages, then, are likely to be more meaningful than measurements on individual nights. That r type E_s ionograms show an increase in virtual height with frequency near the critical frequency indicates reflection from an ionized layer of considerable depth, with a maximum electron density some distance above the bottom of the

layer. Thus if E_{sr} ionization is due to proton precipitation, as diurnal correlations with hydrogen emission indicate, then the proton flux produces a much thicker layer of ionization than that due to electron precipitation. Similarly, the hydrogen emission can be expected to originate from a wider height interval than the visual auroral emissions. This is discussed further in Section VI(e).

The correlation between hydrogen emission and r type E_s provides a way of extrapolating the curve of occurrence of zenith hydrogen emission into the daylight hours, using continuous ionospheric records. Figure 19(b) shows that the occurrence of r type E_s continues to fall in the morning hours and that there is a period of negligible occurrence between 0900 and 1200 U.T. From this it is inferred that the hydrogen emission zone has moved well south of Mawson by 0600 to 0700 U.T., either staying in the south until about 1400 U.T. or falling in intrinsic intensity to a low value between the hours of 0900 and 1200 U.T. These inferences agree very well with the shape of the hydrogen emission zone, as determined with results from the New Zealand stations at Scott and Hallett combined with those already described from Mawson (Eather and Sandford 1966).

(g) Association with Magnetic Variations

The year 1963 was near the minimum of the 11 year sunspot cycle. Therefore, there were very few strong magnetic storms during the year, and in fact the strongest occurred near the summer months when there was insufficient darkness to permit effective hydrogen emission observations. The number of cloudless moonless occasions on which strong magnetic storms occurred during the auroral season was insufficient for any possible dependence of hydrogen emission on magnetic activity to be observed.

There did not appear to be any noticeable changes in behaviour with local K index, at least up to K index values of 6. The local K index depended mainly on the intensity, location, and extent of visual auroras, while, as previously stated, hydrogen emission intensity was not related to visual auroral intensity or visual auroral extent.

Movements of the hydrogen emission zone from south to north, and then from north to south, were not accompanied by any observable magnetic changes. (Changes of 25 gamma would have been readily detected by the fluxgate magnetometer.) It would, nevertheless, be interesting to search for magnetic fluctuations associated with movements of the hydrogen emission zone with a more sensitive magnetometer.

VI. HEIGHT OF THE HYDROGEN EMISSION—LINE PROFILE SHAPE

It was intended to try to measure the height of the hydrogen emission by the van Rhijn method (see Chamberlain 1961 for discussion of this method). However, calculations of the $H\beta$ integrated intensity (Section III) depend on assuming a line profile shape. Published hydrogen line profiles vary considerably, so it was not possible to determine integrated intensities with the accuracy required by the van Rhijn method.

The van Rhijn method was then used "in reverse" to deduce hydrogen line profile shapes, assuming likely emission heights.

(a) The van Rhijn Method

The method makes use of the fact that the precise manner in which the measured intensity of a uniform emitting layer changes with the zenith angle of observation depends on the height of the emitting layer. If I_{ξ} is the intensity measured at a zenith angle ξ , then

$$I_{\xi} = I_0 \left\{ 1 - \left(\frac{a}{a+h} \right)^2 \sin^2 \xi \right\}^{-\frac{1}{2}},$$

where a is the radius of the Earth and h the height of emission. Various corrections must be applied to allow for atmospheric absorption and scattering, ground reflection, wide height extent of the emission, and perhaps latitude dependence of the emission (see Chamberlain 1961).

The method is limited by the condition that the measured intensities must be very accurate, as must the appropriate corrections, to obtain reasonable accuracy in deduced heights.

(b) Application to the Hydrogen Emission

Because the hydrogen emission zone is a wide diffuse region and usually not subject to rapid intensity fluctuations, it seemed that the van Rhijn method might be applicable in the determination of the height of emission. It is, in fact, the diffuse nature of the zone that prevents the use of triangulation techniques of height determination.

The integrated H β intensity as calculated from the photometer records (see Section III) was used, since the directionally dependent Doppler shift precluded the use of central or peak intensity. Unfortunately the integrated intensity depends on the assumed line profile, the exact form of which could not be determined by the tilting-filter techniques. Published hydrogen profiles show wide variations in the $\lambda 4840$ region (the low wavelength side of the profile). The variation of calculated integrated intensity with assumed line profile has not been important in previous discussions, because only relative intensities were of importance. In any case, the variation in relative intensities is only of the order of 20% between the limits of published hydrogen line profiles. This variation, however, makes a considerable difference to calculated heights using the van Rhijn method. Consequently all calculations on van Rhijn height determination were made starting from two different assumed line profiles: those of Zwick and Shepherd (1963) and those of Veissberg (1962). Veissberg (1962) did not publish a magnetic horizon hydrogen line profile, and in fact very few authors have published horizon profiles. Hence it was necessary to assume a magnetic horizon hydrogen line profile to couple with Veissberg's zenith profile. A profile slightly narrower than the horizon profiles of Zwick and Shepherd (1963) and of Johansen and Omholt (1963) was chosen, as Veissberg's zenith profile was much narrower than the zenith profiles of the above authors. The assumed profile was approximately midway between those of Zwick and Shepherd and Johansen and Omholt and that of Chamberlain (1961) (see Fig. 21(b)); thus the assumed profile could have had a half-intensity width that was up to 2 Å in error. This would have little effect on the calculated integrated intensities, as these are dependent on the shape of zenith and "near zenith" profiles in the 4840 Å region.

Various published profiles are shown in Figures 21(a) and 21(b). Zwick and Shepherd's zenith profile shows the highest intensity at 4840 Å, while Veissberg's shows the lowest intensity at this wavelength (neglecting Montalbetti's profile, as the corrections for scattering that he applied in profile measurement are considered to be too uncertain to attach any confidence to his final profile).

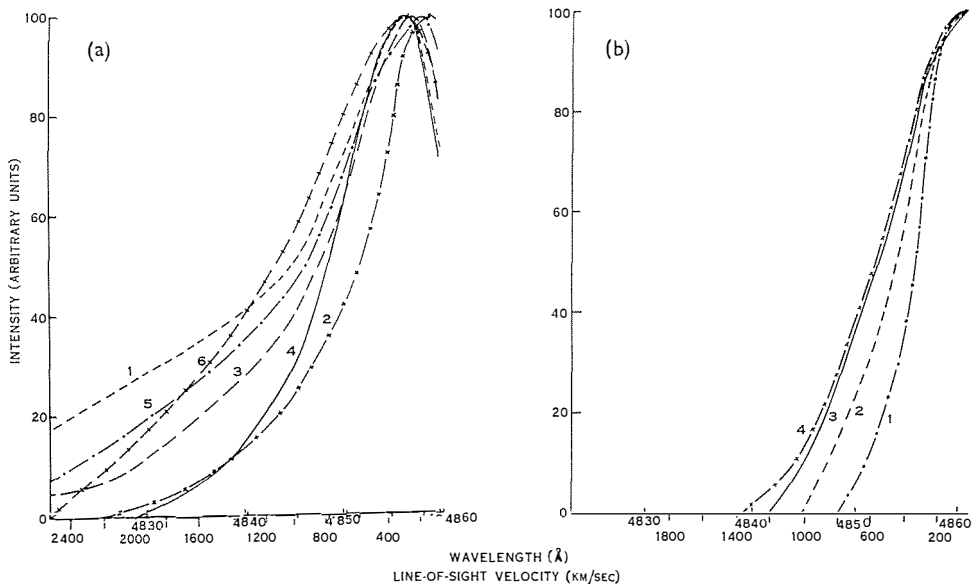


Fig. 21.—(a) Published magnetic zenith hydrogen line profiles: 1 Galperin (1959), 2 Montalbetti (1959), 3 Galperin and Yurchenko (1962), 4 Veissberg (1962), 5 Johansen and Omholt (1963), 6 Zwick and Shepherd (1963). (b) Published magnetic horizon hydrogen line profiles: 1 Chamberlain (1961), 2 assumed Veissberg (1962), 3 Johansen and Omholt (1963), 4 Zwick and Shepherd (1963).

(c) Latitude Corrections

All measurements were made along the eccentric dipole east-west direction, so as to minimize latitude effects. For the same reason, measurements were only made when the hydrogen emission was fairly uniform over the sky. Even so, it was necessary to apply latitude corrections as follows.

Measurements along the east-west direction will correspond to the hydrogen intensity at the latitude of the station, θ_s , for small zenith angles ξ , but at high zenith angles will correspond to the hydrogen intensity at more northern latitudes ($\theta_s - \Delta(\xi)$), where $\Delta(\xi)$ is given by

$$\Delta(\xi) = \theta_s - \sin^{-1} \left[\cos \left\{ \xi - \sin^{-1} \left(\frac{a}{a+h} \sin \xi \right) \right\} \sin \theta_s \right]$$

with h the height of emission and a the radius of the Earth. For Mawson $\theta_s = 71^\circ$ (eccentric dipole latitude) and

$$\begin{aligned} \Delta(\xi) &= 0.13^\circ & \text{for } h = 100 \text{ km, } \xi = 70^\circ, \\ \Delta(\xi) &= 0.98^\circ & \text{for } h = 300 \text{ km, } \xi = 70^\circ. \end{aligned}$$

In practice, the latitude variation of hydrogen emission along the north–south meridian was determined from the north–south scan immediately before the east–west measurements were made. Assuming that the same latitude variation applies along the longitude range of observation, $I(\theta_s - \Delta(\xi))/I(\theta_s)$ was determined over the range of zenith angles 0° – 80° .

$\Delta(\xi)$ depends on the assumed height of emission, as does the procedure for conversion of modulation of the photometer records to integrated $H\beta$ intensities (see Section III). Thus all calculations, including the latitude corrections described above, were carried out for two assumed heights of emission, 100 and 300 km; the experimental van Rhijn curves were then compared with theoretical curves for heights of emission 100 and 300 km.

As can be seen above, $\Delta(\xi)$ varies by a factor of seven between assumed heights of emission of 100 and 300 km; the latitude correction is much less height dependent, as the latitude distribution measured from the north–south scan is also height dependent. The latitude correction varied from zero at low zenith angles to

$$2\% \text{ at } \xi = 70^\circ, \quad h = 100 \text{ km}$$

and

$$3.5\% \text{ at } \xi = 70^\circ, \quad h = 300 \text{ km.}$$

depending, of course, on the actual north–south distribution at the time.

(d) *Experimental van Rhijn Curves—Line Profiles*

The following computational procedure was used: the measured modulation of photometer records was converted to integrated intensity (Section III), assuming

- (1) Zwick and Shepherd's profiles, and
- (2) Veissberg's profiles,

for assumed heights of emission 100 and 300 km. The integrated intensities were then corrected for latitude effects, for the assumed heights of emission. The resulting curves of I_ξ/I_0 against ξ were plotted and compared with Ashburn's (1954) theoretical curves for an atmospheric extinction coefficient of 0.15, and a ground albedo of 0.8 (appropriate for snow cover).

As mentioned earlier, because of the uncertainty in the assumed line profiles, the aim was not to attempt to determine the height of emission, but to find which assumed line profiles gave a reasonable height of emission. A "reasonable" height of emission was taken as 100 to 300 km, limits well confirmed by theoretical luminosity curves for the hydrogen emission (Eather and Burrows 1966).

Figure 22(a) shows the comparison of experimental and theoretical van Rhijn curves for a number of separate scans. It may be seen that Zwick and Shepherd's profiles result in deduced heights that are far too high, regardless of the initial assumptions, whereas Veissberg's profiles give deduced heights in the "reasonable" 100–300 km range. Figure 22(b) shows the average van Rhijn curves from six successful east–west scans.

These results demonstrate the great sensitivity of the $H\beta$ van Rhijn ratio to line-profile shape. This sensitivity, together with the comparative insensitivity to

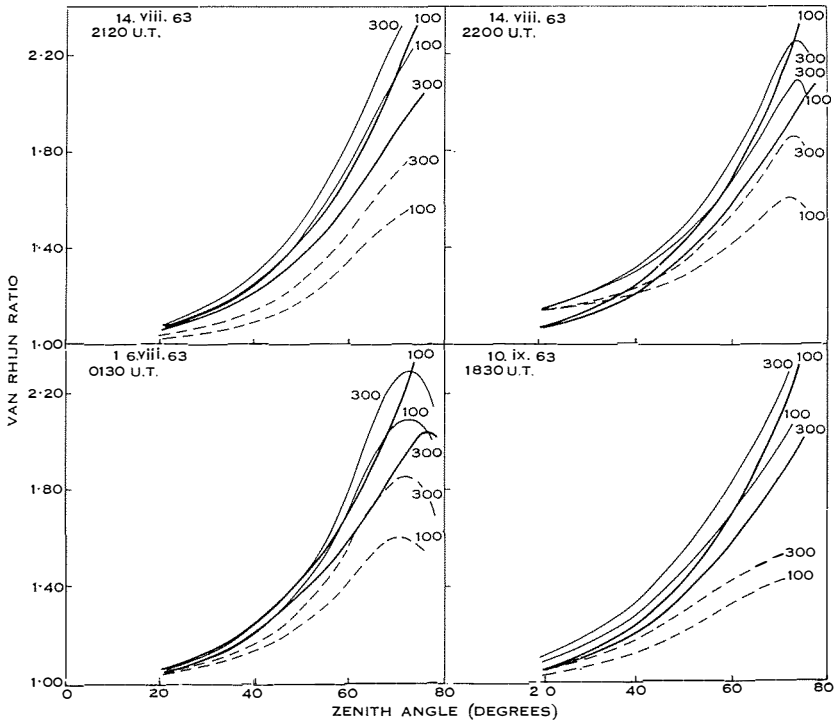


Fig. 22(a).—Comparison of experimental and theoretical van Rhijn curves for assumed heights of emission of 100 and 300 km. ——— Assuming Veissberg's profiles; - - - - assuming Zwick and Shepherd's profiles; ——— theoretical curves (after Ashburn 1954).

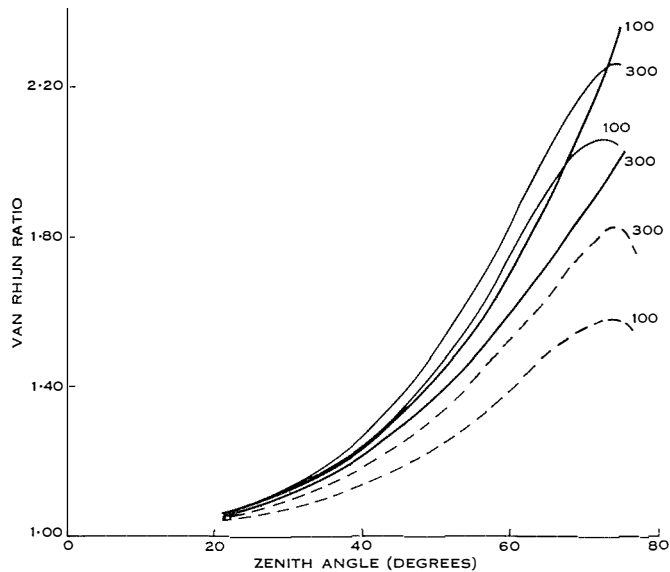


Fig. 22(b).—Average van Rhijn curves for assumed heights of emission of 100 and 300 km (same key as Fig. 22(a)).

emission height, makes the van Rhijn technique particularly suited to the testing of assumed line profiles; the same factors render the technique useless for height determination without accurate line profiles.

It is concluded that the zenith hydrogen line profile published by Veissberg is closest to the actual line profiles from auroral hydrogen emission. Possibly, the high velocity tail of the magnetic zenith profile has been overestimated by other workers owing to contamination from unresolved nitrogen bands. This could explain why all other published profiles have higher intensities at 4840 Å than Veissberg's profile.

It is interesting to compare the ratio of moments of horizon to zenith profiles, derived from the Zwick and Shepherd and Veissberg profiles, with those derived theoretically assuming the incident protons have a pitch angle distribution varying as $\cos^n\theta$. Following Chamberlain (1961, p. 260) this comparison is made in Table 1, which lists the values of n necessary to yield the observed moments.

TABLE 1
VALUES OF n CONSISTENT WITH OBSERVED RATIO \bar{v}_z^m/\bar{v}_2^m

Profile	Ratio of Moments		Derived n	
	$m = 1$	$m = 2$	$m = 1$	$m = 2$
Zwick and Shepherd (1963)				
Corrected	0.35	0.12	4	6
Uncorrected	0.50	0.25	1	2
Veissberg (1962)	0.66	0.60	0	0

Veissberg's profiles thus give consistent results for n , whereas Zwick and Shepherd's do not; the Veissberg n supports the conclusion of Chamberlain (1961) that the proton pitch angle distribution over the upper atmosphere is isotropic.

(e) Asymmetry of Magnetic Horizon Hydrogen Line Profiles

Several authors have published magnetic horizon hydrogen line profiles that are asymmetrical (see, for example, Montalbetti 1959; Zwick and Shepherd 1963); this asymmetry has been attributed to scattering of radiation from the zenith in the lower atmosphere. Consequently, corrections have been made to the horizon profile by subtracting enough of the zenith profile to make it symmetrical. Similar scattering corrections have been applied to the zenith profile by subtracting a fraction of the corrected horizon profile.

However, the scattered-light corrections that have been applied in this manner seem to be impossibly large. Montalbetti, for example, concluded that more than half of the observed zenith profile was due to scattered light from the horizon; Zwick and Shepherd's "corrected" and "uncorrected" profiles suggest that about 20% of the zenith radiation was assumed scattered to the horizon, and vice versa.

This would imply that if a bright visual aurora (say strength 3) covered most of the horizon region of the sky then of the order of 20% of its light should be scattered

to the zenith; that is, there should be an observed brightness in the zenith equivalent to a strength 2 aurora. In fact, one would never observe well-defined visual forms if such high scattering coefficients were operative. Plate 2 shows an all-sky camera photograph of a strong aurora covering most of one-half of the sky, and it is quite obvious that there is little scattering of this light to the other half of the sky; even a rough estimate from this photograph leads to the conclusion that less than 1% of the auroral light is scattered to the other half.

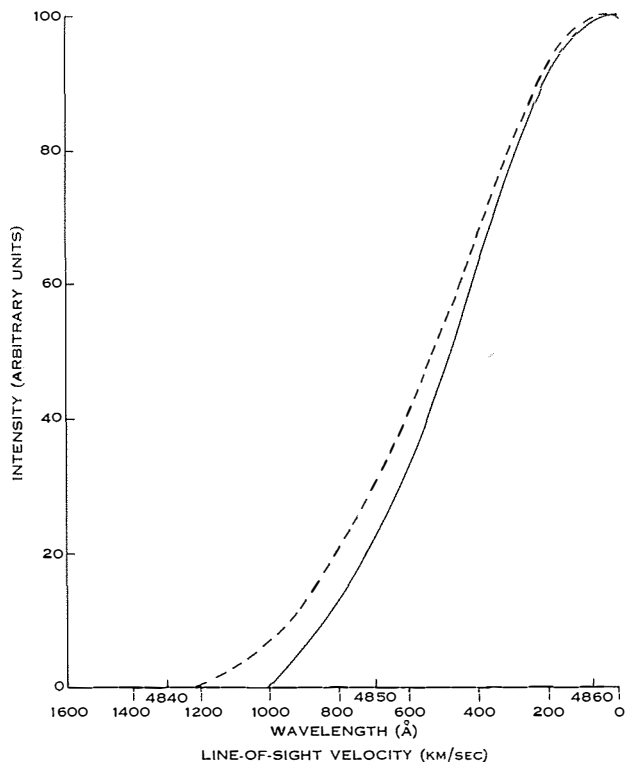


Fig. 23.—Effect of hydrogen emission from a wide height interval (100–300 km) on an assumed (symmetrical) magnetic horizon line profile.
 — Assumed profile for narrow height distribution; - - - derived profile assuming uniform emission from 100–300 km.

There are two possible explanations of the observed asymmetrical, magnetic horizon, hydrogen line profiles.

(1) The asymmetry could be explained by a wide height distribution of the emission. If the observational direction makes an angle of 90° with the field lines at, say, 100 km, then the angle made with the field lines at 300 km will not be 90° . This angle made at 300 km depends on the latitude of the observing station, and for Mawson (73.3° S. geomagnetic) is 82° (calculated for actual field configuration at Mawson). The effect on an assumed symmetrical horizon profile, from uniform

emission between 100 and 300 km, was calculated for Mawson and the resulting asymmetry is shown in Figure 23. The asymmetry due to this effect is of the order of that observed by Montalbetti (1959) and by Zwick and Shepherd (1963). Calculations (Eather and Burrows 1966) suggest that hydrogen emission does in fact cover a much wider height range than does the visual emissions but that the range is not as wide as 200 km; the calculated luminosity profiles suggest that the height distribution of emission might explain about half of the observed horizon profile asymmetry.

(2) Observations may not have been in the exact magnetic horizon direction. To obtain the magnetic horizon direction, a height of emission must first be assumed. This has not been discussed by Montalbetti (1959) or by Zwick and Shepherd (1963). Calculations show that for geomagnetic latitudes greater than 65° , it is not possible to have a direction from the ground that makes an angle of 90° with the field lines at 100 km. Calculations were carried out for a perfect dipole field and local field variations from the dipole will of course affect the result. However, the calculation emphasizes the importance of making such calculations for the location of the observing station and for the actual field configuration at the station. As this point has not been discussed in papers on magnetic horizon hydrogen profiles, the calculations have apparently not been made. Small deviations from the true magnetic horizon direction ($\lesssim 10^\circ$) are sufficient to explain the observed horizon profile asymmetry.

Thus it is quite probable that the above two factors are sufficient to account for reported hydrogen line profile asymmetry in the direction of the magnetic horizon.

VII. THE HYDROGEN EMISSION ZONE

Measurements of the hydrogen emission at Mawson, and measurements at the New Zealand Antarctic stations at Scott and Hallet, have been used to delineate a zone of hydrogen emission for the southern hemisphere. This zone has been published by Eather and Sandford (1966). It is important to note that this zone is one that fits the available data but may only be approximate in the shape of its boundaries. Additional data from stations well distributed in latitude and longitude would be required to determine the shape of the zone boundaries with any more certainty.

VIII. ACKNOWLEDGMENTS

The observations were carried out while one of us (R.H.E.) was a member of the Australian National Antarctic Research Expeditions at Mawson during 1963. We would like to acknowledge the assistance of members of this expedition, especially Mr. D. Creighton, who kept the large amount of electronic equipment operational and gave invaluable assistance in many other ways. Ionospheric data were supplied by Mr. R. Schaeffer of the Ionospheric Prediction Service. We also thank Dr. K. M. Burrows of the University of New South Wales for valuable discussions on this work.

The latter part of the investigation was completed while one of us (R.H.E.) held a CSIRO Post-graduate Studentship at the University of New South Wales.

IX. REFERENCES

- ASHBURN, E. V. (1954).—*J. Atmos. Terr. Phys.* **5**: 83.
- BOND, F. R., and JACKA, F. (1962).—*Aust. J. Phys.* **15**: 261.
- BRICARD, J., and KASTLER, A. (1947).—*Annls Geophys.* **3**: 308.
- BRICARD, J., and KASTLER, A. (1948).—“Emission Spectra of Night Sky and Aurora.” p. 70. (Physical Soc.: London.)
- BRICARD, J., and KASTLER, A. (1950).—*Annls Geophys.* **6**: 286.
- CHAMBERLAIN, J. W. (1961).—“Physics of the Aurora and Airglow.” (Academic Press: New York.)
- DOWDEN, R. L. (1963).—Ionospheric Prediction Service Rep., Hobart.
- EATHER, R. H., and BURROWS, K. M. (1966).—Excitation and ionization by auroral protons. *Aust. J. Phys.* **19**: (in press).
- EATHER, R. H., and JACKA, F. (1966).—*Aust. J. Phys.* **19**: 215.
- EATHER, R. H., and SANDFORD, B. P. (1966).—*Aust. J. Phys.* **19**: 25.
- GALPERIN, YU. I. (1959).—*Planet. Space Sci.* **1**: 57.
- GALPERIN, YU. I. (1963).—*Planet. Space Sci.* **10**: 187.
- GALPERIN, YU. I., and YURCHENKO, O. T. (1962).—Aurora and Airglow. No. 9. (Publishing House “Nauka”: Moscow.)
- GINZBURG, V. L. (1943).—*Dokl. Akad. Nauk. SSSR* **38**: 237.
- HELLIWELL, R. A. (1962).—Proc. Int. Conf. on the Ionosphere, London, July 1962, pp. 452–60.
- HERMAN, L. and BELON, A. E. (1961).—Univ. Alaska Rep. No. Y/22.6/327.
- JOHANSEN, O. E., and Omholt, A. (1963).—*Planet. Space Sci.* **11**: 1223.
- JOHNSON, H. M. (1960).—*Mem. Mt. Stromlo Obs.* Vol. 3, No. 15.
- MALVILLE, J. M. (1960).—*Planet. Space Sci.* **2**: 130.
- MONTALBETTI, R. (1959).—*J. Atmos. Terr. Phys.* **14**: 200.
- PROKUDINA, V. S. (1959).—Spectral, Electrochemical and Radar Researches of Aurora and Airglow. No. 1, p. 43.
- VEGARD, L. (1939).—*Nature* **144**: 1089.
- VEGARD, L. (1955).—*Geofys. Publik.* **19**: 1.
- VEISSBERG, O. L. (1962).—*Aurora and Airglow* **8**: 36.
- YEVLAISHIN, L. S. (1961).—*Geomag. Aeronomy* **1**: 50.
- ZWICK, H. H., and SHEPHERD, G. G. (1963).—*J. Atmos. Terr. Phys.* **25**: 604.